Neurobiology of Disease 121 (2019) 58–64

Contents lists available at ScienceDirect

Neurobiology of Disease

journal homepage: www.elsevier.com/locate/ynbdi

Inactivation of *Magel2* suppresses oxytocin neurons through synaptic excitation-inhibition imbalance

Tayfun Ates[a,1], Merve Oncul[a,1], Pelin Dilsiz[a], Iskalen Cansu Topcu[b], Cihan Civan Civas[b], Muhammed Ikbal Alp[a], Iltan Aklan[b], Edanur Ates Oz[a], Yavuz Yavuz[b], Bayram Yilmaz[b], Nilufer Sayar Atasoy[a], Deniz Atasoy[a,*,2]

[a] Department of Physiology, School of Medicine, Regenerative and Restorative Medical Research Center (REMER), Istanbul Medipol University, Istanbul, Turkey
[b] Department of Physiology, School of Medicine, Yeditepe University, Istanbul, Turkey

ARTICLE INFO

Keywords:
Prader Willi Syndrome
Autism
magel2
Oxytocin
AMPA
NMDA
Electrophysiology

ABSTRACT

Prader-Willi and the related Schaaf-Yang Syndromes (PWS/SYS) are rare neurodevelopmental disorders characterized by overlapping phenotypes of high incidence of autism spectrum disorders (ASD) and neonatal feeding difficulties. Based on clinical and basic studies, oxytocin pathway defects are suggested to contribute disease pathogenesis but the mechanism has been poorly understood. Specifically, whether the impairment in oxytocin system is limited to neuropeptide levels and how the functional properties of broader oxytocin neuron circuits affected in PWS/SYS have not been addressed. Using cell type specific electrophysiology, we investigated basic synaptic and cell autonomous properties of oxytocin neurons in the absence of MAGEL2; a hypothalamus enriched ubiquitin ligase regulator that is inactivated in both syndromes. We observed significant suppression of overall *ex vivo* oxytocin neuron activity, which was largely contributed by altered synaptic input profile; with reduced excitatory and increased inhibitory currents. Our results suggest that dysregulation of oxytocin system goes beyond altered neuropeptide expression and synaptic excitation inhibition imbalance impairs overall oxytocin pathway function.

1. Introduction

Prader Willi Syndrome (PWS) is a complex neurogenetic disorder that involves paternal loss of a chromosomal 15q11.2–13 region, which is imprinted on the maternal copy. Distinctive characteristics of PWS involve defects in social communication, restrictive and repetitive behaviors, difficulty in thriving, poor suckling in neonates followed by lack of satiety and obesity in childhood (Burnside et al., 2011; Dykens and Kasari, 1997; Holm et al., 1993; Milner et al., 2005). In addition, multiple endocrine dysfunctions are common among PWS patients, suggesting involvement of hypothalamus (Swaab, 1997). The pathophysiological mechanism of PWS phenotypes has not been fully elucidated but likely to involve contribution of more than one of the inactivated genes that are defined as *MKRN3, MAGEL2, NDN, NPAP1 and SNURF-SNRPN* and non-coding sno-RNAs. Among these genes, *MAGEL2* is almost exclusively expressed in the hypothalamus (Bittel and Butler, 2005; Hanel and Wevrick, 2001; Schaaf et al., 2013). Remarkably, a PWS-related condition, Schaaf-Yang Syndrome (SYS), is also identified by nonsense mutations in *MAGEL2* gene and display overlapping phenotypes with PWS including autism spectrum disorder (ASD) and early life feeding difficulties (Fountain and Schaaf, 2016).

Defects in oxytocin (OXT) system may contribute to pathogenesis of some of the observed phenotypes in PWS (Kabasakalian et al., 2018). In addition to its functions as a peripheral hormone, OXT is known to be involved in diverse behavioral and physiological functions as social cognition and feeding (Gimpl and Fahrenholz, 2001; Grinevich et al., 2016). Consistently, multiple groups have reported OXT abnormalities in PWS patients. For example, postmortem brain tissue evaluations showed reduced number of OXT producing neurons (Swaab et al., 1995), decreased adult plasma OXT levels and OXTR expression (Hoybye et al., 2003; Bittel et al., 2007) while others reported increased cerebrospinal fluid OXT levels (Martin et al., 1998) and increased plasma OXT levels in PWS children (Johnson et al., 2016). The pathophysiological significance of OXT pathway defects is not well

* Corresponding author at: Istanbul Medipol University, School of Medicine, REMER, Ekinciler Cd. No 19 Beykoz, Istanbul, Turkey.
E-mail address: datasoy@medipol.edu.tr (D. Atasoy).
[1] These authors contributed equally to this work.
[2] Present address: Department of Pharmacology, Roy J. and Lucille A. Carver College of Medicine, University of Iowa, Iowa City, Iowa.

https://doi.org/10.1016/j.nbd.2018.09.017
Received 3 August 2018; Received in revised form 3 September 2018; Accepted 17 September 2018
Available online 19 September 2018
0969-9961/

understood but these abnormalities can be recapitulated in animal models of PWS as well. *Magel2* deficient mice display defects in OXT processing and maturation neonatally. Interestingly, early onset feeding difficulties as well as social defects are also recapitulated in this mice, which can be rescued by OXT treatment (Schaller et al., 2010; Fountain et al., 2017). In addition, the oxytocin levels appear to be restored and indeed increased later in adulthood (Meziane et al., 2015).

Although the existing studies clearly point toward OXT system abnormalities in PWS patients and mouse models, much of these reports rely on peptide or mRNA expression level measurements. On the other hand, OXT is a signaling molecule that functions in the context of a broader circuit that is composed of OXT-expressing neurons and their connections. The impact of PWS-SYS mutations on the functional circuit properties of OXT neuron circuits has not been addressed. Here we used a *Magel2* deficient mouse model of PWS-SYS to investigate synaptic and cell autonomous properties of OXT neurons. Our results showed that OXT neuron dependent impairment goes beyond peptide expression levels with drastic alterations in excitation/inhibition balance such that reduced excitation and increased inhibitory input suppresses overall OXT neuron activity.

2. Methods

2.1. Animals

All animal care, maintenance and experimental procedures were approved by Istanbul Medipol University Animal Care and Use Committee (MEDITAM). Mice were housed at 22 °C–24 °C on a 12-h light (06:00) and dark (18:00) cycle with *ad libitum* access to water and standard mouse chow unless otherwise noted. Magel inactivated C57BL/6-*Magel2*^{tm1Stw}/J (Jackson Labs Stock 009062) line and oxytocin-neuron specific cre recombinase-expressing line B6;129S-*Oxt*$^{tm1.1(cre)Dolsn}$/J (Jackson Labs Stock 024234) were used in the experiments and the lines were maintained through mating with C57BL/6 background. Male mice carrying *Magel2*-null copy were crossed to *Oxt-cre* female mice to generate *Magel2*$^{m+/p-}$::*Oxt-cre* double transgenic mice. For control, *Magel2*$^{m+/p+}$::*Oxt-cre* littermates were used. Experiments were done with 5–7 weeks old, age-matched littermate female and male mice.

2.2. Stereotaxic rAAV injections

Cre dependent EGFP expressing rAAV vector was purchased from http://www.addgene.org/. *rAAV2/8-FLEX-EGFP* (8×10^{13} genomic copies/ml) was produced and purified as described previously (Mathews et al., 2002). P35-P45 mice were anaesthetized with isoflurane on a stereotaxic instrument (David Kopf instruments, Tujunga-CA) for stereotaxic rAAV injections (Atasoy et al., 2012). Scalp was incised to expose the skull for drilling. A total of 250 nl of rAAV was injected using a pulled glass pipette (Drummond Scientific, Wiretrol, Broomall-PA) with 40–50 µm tip diameter. Injections were targeted to paraventricular nucleus of hypothalamus (PVH) using the coordinates, bregma: −0.80 mm, midline: ± 0.25 mm, dorsal surface −5.00 mm. 20 nl/min injection speed was controlled by a micromanipulator (Narishige, East Meadow, NY). The pipette was withdrawn to finalize the injection. The scalp was stitched carefully and mice were allowed 2 weeks for recovery and transgene expression.

2.3. Electrophysiology

For *ex vivo* recordings, P45-P60 female and male mice were used. After viral infection, mice were deeply anaesthetized with isoflurane and decapitated. Coronal brain slices (300 µm thickness) containing the PVH were sectioned using vibratome (Leica VT1000S). Slices were prepared in chilled cutting solution containing (in mM): 234 sucrose, 28 $NaHCO_3$, 7 dextrose, 2.5 KCl, 7 $MgCl_2$, 0.5 $CaCl_2$, 1 sodium ascorbate, 3 sodium pyruvate and 1.25 NaH_2PO_4, aerated with 95% O_2/5% CO_2. Slices were transferred to artificial cerebrospinal fluid (aCSF) containing (in mM): 119 NaCl, 25 $NaHCO_3$, 11 D-glucose, 2.5 KCl, 1.25 $MgCl_2$, 2 $CaCl_2$ and 1.25 NaH_2PO_4, aerated with 95% O_2/5% CO_2. Slices were incubated (30 min) at room temperature (20–24 °C) and then maintained and recorded at same conditions. The neurons were identified and targeted by green fluorescence emission and were patched using pipettes with 4–5 MΩ tip resistances in the bath when filled with an internal solution. The recordings were obtained using pipettes (Harvard Apparatus) made from borosilicate glass capillaries pulled on a Flaming-Brown micropipette puller (Model P-1000, Sutter Instruments, Novato, CA). Loose-seal, recordings (aCSF internal) were made in voltage clamp mode with holding current maintained at zero in the absence of any blockers, most neurons fired spontaneously. Whole cell voltage-clamp recordings were performed for spontaneous excitatory postsynaptic currents (sEPSCs) and spontaneous inhibitory postsynaptic currents (sIPSCs) in the presence of $GABA_A$ (PTX 10 µM) and glutamate receptor blockers CNQX (10 µM) + AP5 (50 µM) respectively. Pipette solution contained (in mM): 125 CsCl, 5 NaCl, 10 HEPES, 0.6 EGTA, 4 Mg-ATP, 0.3 Na_2GTP, 10 lidocaine N-ethyl bromide (QX-314), pH 7.35 and 290 mOsm. The holding potential was set to −60 mV. To measure paired-pulse ratio (PPR), whole cell voltage-clamp recordings were performed in the presence of $GABA_A$ or glutamate receptor blockers to isolate evoked EPSC and IPSC. Electrical stimulation performed using a field electrode that was placed within adjacent to the third ventricle of PVH to activate the ascending fiber tract. Half-maximal stimulus strength was used for PPR measurements, we waited at least 30 s between successive field stimuli. For NMDA/AMPA ratio, AMPAR response was quantified as the peak negative current at a holding potential of −60 mV, the NMDAR response was quantified using a holding potential of +40 mV, and to quantify NMDA current amplitude, 50 ms post-stimulation point was measured. For current clamp recordings, a potassium gluconate based internal solution was used. Pipette solution contained (in mM): 145 K-gluconate, 1 $MgCl_2$, 10 HEPES, 1.1 EGTA, 2 Mg-ATP, 0.5 Na_2-GTP, and 5 Na_2-phosphocreatine (pH 7.3 with KOH; 290–295 mOsm). Recordings were corrected for liquid junction potential. Current injection protocol was set for 200 ms pulses of 20 pA steps starting from −40 pA to +140 pA.

2.4. Imaging

Mice were transcardially perfused with 4% paraformaldehyde in 0.1 M phosphate buffer fixative (pH 7.4). Brains were removed and transferred to the same fixative solution for 4 h. 75 µm brain sections were sliced with vibratome, transferred to microscope slides and mounted with Fluoromount (Sigma F4680). Imaging was performed by confocal microscopy (Zeiss). For spine quantification, basal dendrites were imaged and analysed double blindly.

2.5. Statistical analysis

The results were represented as means ± SEM. To assess the significance between *Oxt-cre* and *Oxt-cre::Magel2*$^{+m/-p}$ (*DTG*) student's *t*-test was used.

3. Results

3.1. Suppressed OXT neuron activity in Magel2 deficient mice

While the existing literature suggests possible involvement of OXT related defects in PWS/SYS phenotypes, our understanding of its mechanism is limited to OXT or OXTR expression levels and virtually nothing is known about the functional profile of these neurons in disease condition. Here we used *Magel2* deficient mouse model of PWS/SYS, an overlapping gene inactivated in both conditions, to dissect out its functional role in OXT neurons. In order to gain selective access to

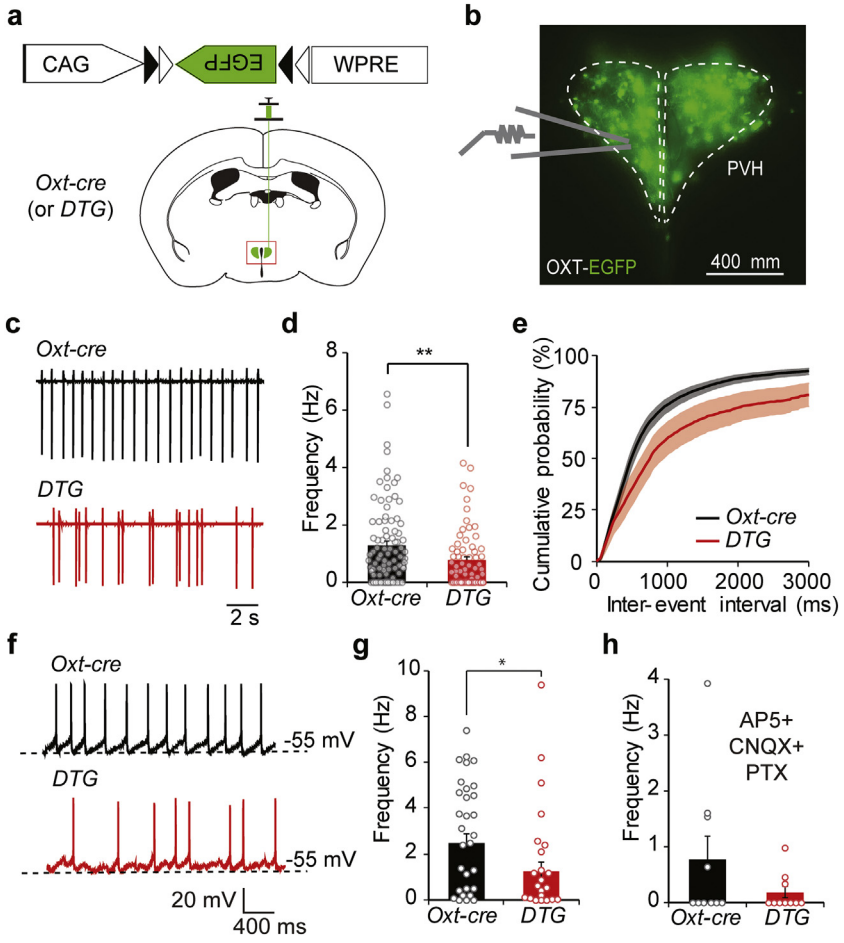

Fig. 1. OXT neuron activity is suppressed in *Magel2*-deficient mice. (a) Schematic drawing for cre-dependent rAAV expression of EGFP in OXT neurons. (b) Photomicrograph of EGFP labeled OXT neurons in paraventricular hypothalamic nucleus (PVH). (c) Representative traces of *ex vivo* loose seal recordings of action currents from OXT neurons of *Oxt-cre* and *Oxt-cre::Magel2*$^{+m/-p}$ (double transgenic: *DTG*) mice. (d) Summary graph for spontaneous spike frequency of OXT neurons (*Oxt-cre*: 1.26 ± 0.15 Hz, n = 94 neurons from 7 mice and *DTG*: 0.71 ± 0.11 Hz, n = 76 neurons from 5 mice; p = .0046). (e) Cumulative probability distribution plot of inter-event interval times for spontaneous activity of OXT neurons that displayed spikes. Shaded areas represent SEM. (f) Representative traces of current clamp recordings of spontaneous action potentials from OXT neurons of *Oxt-cre* and *DTG* mice. (g) Summary graph for spontaneous action potential firing rate of OXT neurons (*Oxt-cre*: 2.45 ± 0.40 Hz, n = 36 neurons from 6 mice and *DTG*: 1.23 ± 0.39 Hz, n = 31 neurons from 5 mice; p = .03). (h) Summary graph for spontaneous action potential firing rate of OXT neurons in the presence of synaptic blockers (AP5, CNQX and PTX) (*Oxt-cre*: 0.77 ± 0.40 Hz, n = 10 neurons from 2 mice and *DTG*: 0.17 ± 0.10 Hz, n = 10 neurons from 2 mice; p = .17). (*p < .05, **p < .01).

OXT neurons, we crossed *Magel2* heterozygous males with *Oxytocin-cre* (*Oxt-cre*) females and used *Magel2*$^{m+/p+}$*::Oxt-cre* (referred as *Oxt-cre* henceforth) and their *Magel2*-deficient littermates *Magel2*$^{m+/p-}$*::Oxt-cre* (referred as double transgenic: *DTG*). We labeled OXT neurons through injection of a cre-dependent fluorophore expressing virus, *rAAV2-FLEX-EGFP* into the paraventricular hypothalamus. Following 2 weeks of EGFP expression, we prepared acute coronal brain slices and performed electrophysiological recordings from OXT neurons (Fig. 1a and b). We first evaluated basic firing and membrane properties. Loose-seal recordings, in which the internal milieu of neurons remain relatively intact, revealed a significant decrease in baseline firing rates of *DTG* OXT neurons (Fig. 1c-e). To better understand the underlying reasons for decreased activity levels, we performed whole cell current clamp recordings. Consistent with loose seal measurements, under whole cell configuration *Magel2* deficient OXT cells showed reduced frequency of action potentials. Interestingly the difference in firing rates was largely abolished when blockers of synaptic transmission were applied to the bath, suggesting that synaptic inputs may contribute to the observed change (Fig. 1f-h and *Oxt-cre*; no blocker: 2.45 ± 0.40 Hz, blocker: 0.77 ± 0.40 Hz, p = .04; *DTG*; no blocker: 1.23 ± 0.39 Hz, blocker: 0.17 ± 0.10 Hz, p = .14).

3.2. Membrane properties of oxytocin neurons in Oxt-cre and DTG mice are similar

OXT neurons might have reduced activity due to higher AP threshold or reduced excitability. To address this possibility, we next measured the baseline resting membrane potential and firing threshold in the absence of any blockers, which were comparable between wild type and *Magel2* deficient OXT neurons (Fig. 2a-c). An examination of excitability profile also showed that there were no significant alterations to basic membrane properties such as number and latency for APs, I–V relationship as well as after hyperpolarization (Fig. 2d-h). These results suggest that basic excitability properties are comparable between genotypes and may not account for decreased activity levels in *Magel2* deficient OXT neurons.

3.3. Balance of synaptic input onto oxytocin neurons is altered

Since the addition of synaptic blockers abolished firing rate differences, we next considered the possibility that alterations in synaptic drive may cause underactivity in OXT neurons of *DTG* mice. To address this possibility, we isolated and measured synaptic currents under whole cell voltage clamp configuration. We observed a significant reduction in the frequency of excitatory spontaneous synaptic current (sEPSC) events with no apparent decrease in event amplitude (Fig. 3a-e). On the contrary, no significant change was observed for spontaneous inhibitory synaptic event (sIPSC) frequency, but median amplitude of events was significantly higher in *DTG* OXT neurons (Fig. 3f-j).

3.4. Selective reduction of AMPA-R dependent currents in Magel2 deficient oxytocin neurons

Altered synaptic input may be caused by a change in the release probability of existing synapses, abundance of synaptic inputs, or a combination of these two. To distinguish between these possibilities, we first quantified release probability of excitatory and inhibitory synaptic inputs. We performed paired pulse stimulation protocol to investigate possible alterations to release probability. Recordings from OXT neurons by paired stimulation protocols across various inter pulse intervals

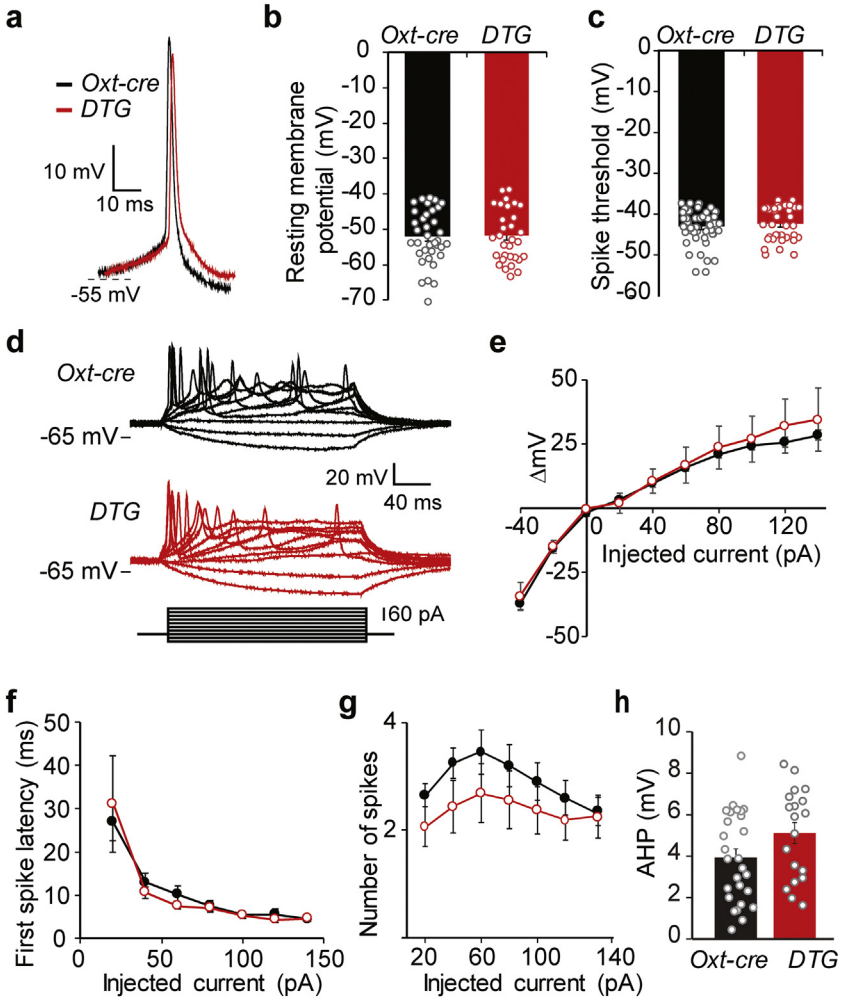

Fig. 2. Excitability properties of OXT neurons are not affected in *Magel2*-deficient mice. (a) Representative action potential traces from OXT neurons of *Oxt-cre* and *DTG* mice. (b) Resting membrane potential graph of OXT neurons (*Oxt-cre*: −52.40 ± 1.26 mV, n = 36 neurons from 6 mice and *DTG*: −52.13 ± 1.33 mV, n = 31 neurons from 5 mice; p = .88). (c) Summary graph for spike threshold (*Oxt-cre*: −43.0 ± 0.79 mV, n = 27 neurons from 6 mice and *DTG*: −42.4 ± 0.95 mV, n = 19 neurons from 5 mice; p = .61). (d) I−V relationship in response to step current injection. Voltage deflections (mV) are shown following 10 consecutive pulses of 20 pA current injections from −40 to +140 pA. (e-g) Summary graphs for I−V relation, AP latency and spike numbers in response to current injections in OXT neurons (*Oxt-cre*: n = 20 neurons from 3 mice and *DTG*: n = 16 neurons from 2 mice). (h) Summary graph for after hyperpolarization values (*Oxt-cre*: 3.93 ± 0.42 mV; *DTG*: 5.11 ± 0.50 mV, p = .08).

suggests that for both excitatory and inhibitory synapses there were no significant change in the paired pulse ratio (Fig. 4a and b). Consistent with the spontaneous activity measurements, evaluation of absolute values half-maximal stimulus-strength evoked currents revealed significant reduction in eEPSCs (*Oxt-cre*: 121.5 ± 23.5 pA, *DTG*: 58.4 ± 9.4 pA, p = .01) and significant increase in eIPSCs values (*Oxt-cre*: 291.8 ± 47.3 ms, *DTG*: 597.2 ± 101.8 ms, p = .007).

We next explored whether the decreased sEPSC frequency was caused by a reduction in the total number of synapses. For this, we evaluated spine numbers, onto which the majority of excitatory synapses are formed, on OXT neuronal dendrites (Arellano et al., 2007). Quantification of confocal images revealed that there were no reductions in the number of spiny protrusions from basal OXT neuronal dendrites of *DTG* mice. On the contrary, *DTG* OXT neuronal dendrites were mildly hypertrophic in terms of spine numbers, but this rise was not statistically significant (Fig. 5a and b). These data show a selective reduction in excitatory drive onto oxytocin neurons which does not appear to be due to decreased synapse number or reduced release efficacy.

Interestingly, electrophysiological and morphological data suggest that even though excitatory synapses may be physically present, as judged by spine count, and their presynaptic release probabilities are comparable, the postsynaptic currents they generate are lower in frequency. This could be explained if some of the *DTG* oxytocin neuronal synapses completely lack the proper postsynaptic machinery to transmit glutamatergic current; a condition that is reminiscent of "silent" synapses during development. If this is the case, we would expect an increase in the ratio of NMDA/AMPA receptor dependent currents. We directly tested this by measuring relative contribution of evoked NMDAR dependent and AMPAR dependent currents. Consistently, NMDA/AMPA ratio was significantly higher in *DTG* OXT neurons compared to littermates (Fig. 5c and d), suggesting a selective loss of AMPA dependent currents from synapses onto OXT neurons from *Magel2*-deficient mice.

4. Discussion

Patients of both Prader-Willi and Schaaf-Yang Syndromes share common phenotypes including high prevalence of autism, neonatal hypotonia and feeding difficulties (Fountain and Schaaf, 2016; Fountain Jr and Schaaf, 2015). Due its extensively studied role in social learning and feeding as well as the reported defects in OXT system in basic and clinical studies, we hypothesized that OXT neuron circuits may underperform in *Magel2* deficiency. Notably, our results showed significant suppression in *ex vivo* activity levels of these key neurons which was not depend on altered membrane properties. Combined addition of synaptic blockers for GABAergic and glutamatergic transmission was effective in significantly reducing activity levels of naïve Oxt neurons but not *Magel2* deficient ones, suggesting a net loss of excitatory drive in mutant mice. Consistently, investigation of synaptic input profile uncovered significant reduction in excitatory drive that is more pronounced for AMPARs, and an increase in inhibitory currents; both of which are likely to contribute to overall suppression of OXT system.

Both presynaptic and postsynaptic mechanisms may underlie the observed alterations in synaptic communication. MAGEL2 is known to

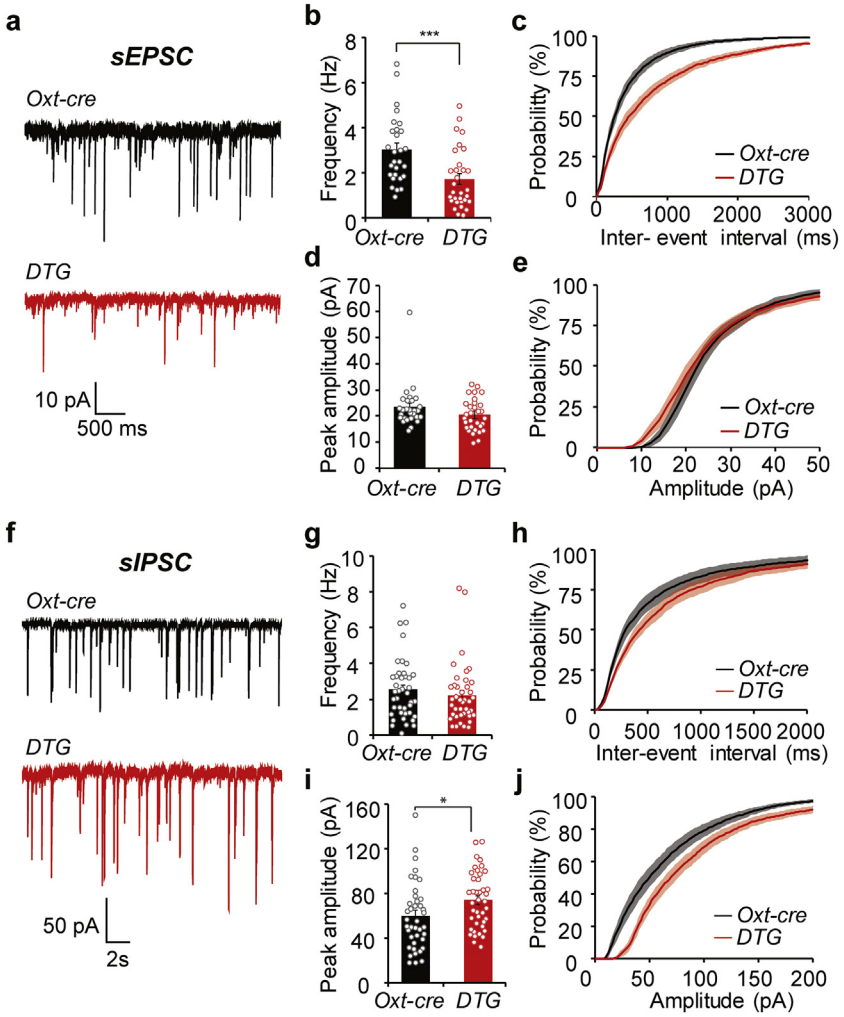

Fig. 3. Altered synaptic inputs onto OXT neurons. (a) Representative traces of spontaneous excitatory postsynaptic currents (sEPSC) recordings. (b) Summary graph for excitatory synaptic activity frequency (*Oxt-cre*: 3.02 ± 0.28 Hz, n = 28 neurons from 4 mice and *DTG*: 1.70 ± 0.23 Hz, n = 31 neurons from 4 mice; p = .0006). (c) Cumulative probability distribution plot of inter-event intervals for excitatory synaptic activity. Shaded areas represent SEM. (d) Peak amplitude graph for excitatory synaptic currents of OXT neurons (*Oxt-cre*: 23.43 ± 1.53 pA, n = 28 neurons from 4 mice and *DTG*: 20.43 ± 1.09 pA, n = 31 neurons from 4 mice; p = .11). (e) Cumulative probability distribution plot of peak amplitudes. Shaded areas represent SEM. (f) Representative traces of spontaneous inhibitory postsynaptic currents (sIPSC). (g) Summary graph for inhibitory postsynaptic current frequency (*Oxt-cre*: 2.53 ± 0.26 Hz, n = 41 neurons from 6 mice and *DTG*: 2.21 ± 0.26 Hz, n = 41 neurons from 6 mice; p = .39). (h) Cumulative probability distribution plot of inter-event intervals for inhibitory synaptic events. Shaded areas represent SEM. (i) Summary graph for peak amplitudes of inhibitory posysynaptic currents (*Oxt-cre*: 60.02 ± 4.64 pA, n = 41 neurons from 6 mice and Oxt-*cre::Magel2*$^{+m/-p}$: 73.90 ± 3.94 pA, n = 41 neurons from 6 mice; p = .02). (j) Cumulative probability distribution plot of peak amplitudes for inhibitory synaptic activity. Shaded areas represent SEM. (*p < .05; ***p < .001).

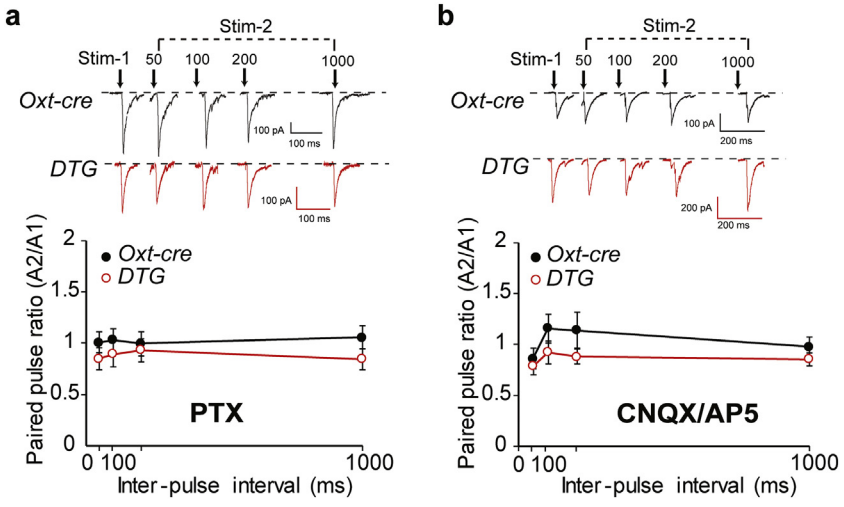

Fig. 4. Synaptic release probability onto OXT neurons is not altered in *Magel2*-deficient mice. (a) Representative paired pulse EPSCs at indicated inter-pulse intervals. Mean paired pulse ratio (PPR) is plotted as a function of inter-pulse interval (*Oxt-cre*: n = 25 neurons from 5 mice and *DTG*: n = 28 neurons from 4 mice). (b) Representative paired pulse IPSCs at indicated inter-pulse intervals. Mean paired pulse ratio (PPR) is plotted as a function of inter-pulse interval (*Oxt-cre*: n = 28 neurons from 5 mice and *DTG*: n = 24 neurons from 5 mice).

be expressed in hypothalamus (Lee et al., 2003), but at cellular level, it is not known whether adult brain OXT neurons contain the protein. While its precise cellular function is still under investigation, MAGEL2 is known to belong MAGE family of ubiquitin ligase regulators (Tacer and Potts, 2017), and it is suggested to form a tripartite complex with E3 ubiquitin ligase and USP7 deubiquitinating enzyme (Hao et al., 2013). This complex interacts with endosomal retromer and activate WASH actin nucleation promoting factor which plays a key role in trafficking and sorting of membrane proteins, including receptors (van der Sluijs and Hoogenraad, 2011; Zhang et al., 2012). Of note, patients with mutations in USP7 have been identified, that also display high incidence of ASD and hypotonia, suggesting that this axis play a critical role in development (Hao et al., 2015). Within OXT neurons MAGEL2 associated complex could be involved in neurotransmitter receptor containing endosomal trafficking. A premise for such a receptor trafficking function has recently been shown for another membrane

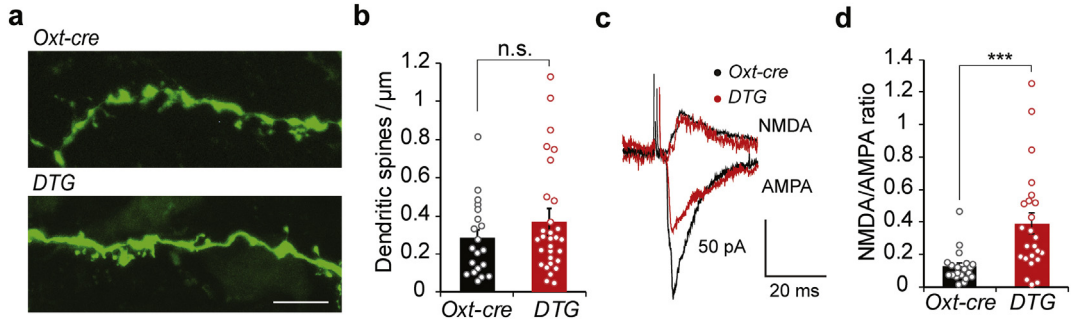

Fig. 5. Reduced AMPAR currents on OXT neurons of *Magel2*-deficient mice. (a) Representative confocal images of OXT neuron dendritic segments. Scale bar, 5 µm. (b) Dendritic spine density graph of OXT neurons (*Oxt-cre*: 0.28 ± 0.04 spines/µm dendrite, n = 27 dendritic branch segments from 4 mice and *DTG*: 0.36 ± 0.07 spines/µm dendrite, n = 30 dendritic branch segments from 3 mice; p = .24). (c) Representative traces from whole-cell voltage-clamp recordings showing NMDAR and AMPAR-mediated currents recorded from OXT neurons of *Oxt-cre* and *DTG* mice. (d) Summary graph for NMDAR/AMPAR current ratio of OXT neurons (*Oxt-cre*: 0.12 ± 0.02, n = 20 neurons from 3 mice and *DTG*: 0.38 ± 0.06, n = 24 neurons from 3 mice; p = .0009). (***p < .001).

protein, leptin receptor (Wijesuriya et al., 2017). Interestingly, our findings on dendritic morphology and NMDA/AMPA ratio suggest that a subset of synapses may completely lack AMPAR, which could explain the decrease in sEPSC frequency without a significant change in event amplitude. This is reminiscent of silent synapses, which are normally common during development but disappear or unsilenced during critical periods (Hanse et al., 2013). Further research is warranted to test the interesting possibility that MAGEL2 endosomal trafficking regulator might be required for proper "unsilencing" of a subset of synapses during development.

Alternatively, impaired synaptic drive may not be a cell autonomous effect, instead, could reflect inability of MAGEL2 deficient presynaptic partners to form or maintain connections. Indeed, *Magel2* deficient mice display defects in development of inputs into paraventricular hypothalamic nucleus (Maillard et al., 2016). Finally, the observed synaptic phenotype might be secondary to other defects observed in these mice such as impaired OXT processing. Especially during early development but also in mature brain, OXT is directly involved in dendrite remodeling and modulation of excitatory synapse development and function (Ferri and Flanagan-Cato, 2012; Jo et al., 1998; Ninan, 2011; Ripamonti et al., 2017). Extensive dendritic release that takes place in OXT neurons (Ludwig and Leng, 2006) may act on the OXT autoreceptors to modulate development and functioning of glutamatergic synapses (Freund-Mercier and Stoeckel, 1995). In addition, our measurements of spontaneous and evoked inhibitory currents uncovered a clear potentiation. Lack of increase in sIPSC frequency suggests that it is not the abundance of inhibitory synapses but rather amount of GABAergic receptors in each synapse may underlie the observed enhancement. This could be due to a failed membrane GABAR removal related to MAGEL2 endosomal function or alternatively a phenotype secondary to overall circuit function.

Notwithstanding the mechanism, our data provide evidence for suppression of OXT system at functional level in a mouse model of PWS-SYS. These results open a new direction of research on possible pre- and postsynaptic means by which synaptic currents are modulated by MAGEL2 ubiquitin ligase regulator. Our results also suggest that despite the reported restoration in oxytocin levels in adulthood, oxytocin neuron defects at circuit level persists. It is possible that MAGEL2 deficiency during development might permanently alter these circuits, alternatively, continued presence of MAGEL2 might be required for proper oxytocin circuit function. While a number of PWS-SYS and ASD mouse models have been characterized for OXT function so far, much of the work have focused on behavioral and neuropeptide level defects. Our approach to dissect OXT system at the level of cellular physiology uncovered previously unsuspected synaptic impairment and provided fresh insight into PWS-SYS pathophysiology. These results also highlight the importance of cell type specific approach, which would help place synaptic pathology into circuit context. Better understanding of precise synaptic mechanisms by which OXT circuits are dysregulated will help design more informed clinical approaches for treatment.

Conflict of interest

The authors declare no competing financial interests.

Acknowledgements

This work is supported by The Scientific and Technological Research Council of Turkey (TUBITAK) funding to D.A. grant no: 214S361.

References

Arellano, J.I., Benavides-Piccione, R., Defelipe, J., Yuste, R., 2007. Ultrastructure of dendritic spines: correlation between synaptic and spine morphologies. Front. Neurosci. 1 (1), 131–143.
Atasoy, D., Betley, J.N., Su, H.H., Sternson, S.M., 2012. Deconstruction of a neural circuit for hunger. Nature 488 (7410), 172–177.
Bittel, D.C., Butler, M.G., 2005. Prader-Willi syndrome: clinical genetics, cytogenetics and molecular biology. Expert Rev. Mol. Med. 7 (14), 1–20.
Bittel, D.C., Kibiryeva, N., Sell, S.M., Strong, T.V., Butler, M.G., 2007. Whole genome microarray analysis of gene expression in Prader-Willi syndrome. Am. J. Med. Genet. A 143A (5), 430–442.
Burnside, R.D., Pasion, R., Mikhail, F.M., Carroll, A.J., Robin, N.H., Youngs, E.L., et al., 2011. Microdeletion/microduplication of proximal 15q11.2 between BP1 and BP2: a susceptibility region for neurological dysfunction including developmental and language delay. Hum. Genet. 130 (4), 517–528.
van der Sluijs, P., Hoogenraad, C.C., 2011. New insights in endosomal dynamics and AMPA receptor trafficking. Semin. Cell Dev. Biol. 22 (5), 499–505.
Dykens, E.M., Kasari, C., 1997. Maladaptive behavior in children with Prader-Willi syndrome, down syndrome, and nonspecific mental retardation. Am. J. Ment. Retard. 102 (3), 228–237.
Ferri, S.L., Flanagan-Cato, L.M., 2012. Oxytocin and dendrite remodeling in the hypothalamus. Horm. Behav. 61 (3), 251–258.
Fountain Jr., M.D., Schaaf, C.P., 2015. MAGEL2 and oxytocin-implications in Prader-Willi Syndrome and beyond. Biol. Psychiatry 78 (2), 78–80.
Fountain, M.D., Schaaf, C.P., 2016. Prader-Willi syndrome and schaaf-yang syndrome: neurodevelopmental diseases intersecting at the MAGEL2 gene. Diseases 4 (1).
Fountain, M.D., Tao, H., Chen, C.A., Yin, J., Schaaf, C.P., 2017. Magel2 knockout mice manifest altered social phenotypes and a deficit in preference for social novelty. Genes Brain Behav. 16 (6), 592–600.
Freund-Mercier, M.J., Stoeckel, M.E., 1995. Somatodendritic autoreceptors on oxytocin neurones. Adv. Exp. Med. Biol. 395, 185–194.
Gimpl, G., Fahrenholz, F., 2001. The oxytocin receptor system: structure, function, and regulation. Physiol. Rev. 81 (2), 629–683.
Grinevich, V., Knobloch-Bollmann, H.S., Eliava, M., Busnelli, M., Chini, B., 2016. Assembling the puzzle: pathways of oxytocin signaling in the brain. Biol. Psychiatry 79 (3), 155–164.
Hanel, M.L., Wevrick, R., 2001. The role of genomic imprinting in human developmental disorders: lessons from Prader-Willi syndrome. Clin. Genet. 59 (3), 156–164.
Hanse, E., Seth, H., Riebe, I., 2013. AMPA-silent synapses in brain development and pathology. Nat. Rev. Neurosci. 14 (12), 839–850.
Hao, Y.H., Doyle, J.M., Ramanathan, S., Gomez, T.S., Jia, D., Xu, M., et al., 2013. Regulation of WASH-dependent actin polymerization and protein trafficking by ubiquitination. Cell 152 (5), 1051–1064.
Hao, Y.H., Fountain Jr., M.D., Fon Tacer, K., Xia, F., Bi, W., Kang, S.H., et al., 2015. USP7

acts as a molecular rheostat to promote WASH-dependent endosomal protein recycling and is mutated in a human neurodevelopmental disorder. Mol. Cell 59 (6), 956–969.
Holm, V.A., Cassidy, S.B., Butler, M.G., Hanchett, J.M., Greenswag, L.R., Whitman, B.Y., et al., 1993. Prader-Willi syndrome: consensus diagnostic criteria. Pediatrics 91 (2), 398–402.
Hoybye, C., Barkeling, B., Espelund, U., Petersson, M., Thoren, M., 2003. Peptides associated with hyperphagia in adults with Prader-Willi syndrome before and during GH treatment. Growth Hormone IGF Res. 13 (6), 322–327.
Jo, Y.H., Stoeckel, M.E., Freund-Mercier, M.J., Schlichter, R., 1998. Oxytocin modulates glutamatergic synaptic transmission between cultured neonatal spinal cord dorsal horn neurons. J. Neurosci. 18 (7), 2377–2386.
Johnson, L., Manzardo, A.M., Miller, J.L., Driscoll, D.J., Butler, M.G., 2016. Elevated plasma oxytocin levels in children with Prader-Willi syndrome compared with healthy unrelated siblings. Am. J. Med. Genet. A 170 (3), 594–601.
Kabasakalian, A., Ferretti, C.J., Hollander, E., 2018. Oxytocin and Prader-Willi syndrome. Curr. Top. Behav. Neurosci. 35, 529–557.
Lee, S., Walker, C.L., Wevrick, R., 2003. Prader-Willi syndrome transcripts are expressed in phenotypically significant regions of the developing mouse brain. Gene Express. Patterns 3 (5), 599–609.
Ludwig, M., Leng, G., 2006. Dendritic peptide release and peptide-dependent behaviours. Nat. Rev. Neurosci. 7 (2), 126–136.
Maillard, J., Park, S., Croizier, S., Vanacker, C., Cook, J.H., Prevot, V., et al., 2016. Loss of Magel2 impairs the development of hypothalamic Anorexigenic circuits. Hum. Mol. Genet. 25 (15), 3208–3215.
Martin, A., State, M., Anderson, G.M., Kaye, W.M., Hanchett, J.M., McConaha, C.W., et al., 1998. Cerebrospinal fluid levels of oxytocin in Prader-Willi syndrome: a preliminary report. Biol. Psychiatry 44 (12), 1349–1352.
Mathews, L.C., Gray, J.T., Gallagher, M.R., Snyder, R.O., 2002. Recombinant adeno-associated viral vector production using stable packaging and producer cell lines. Methods Enzymol. 346, 393–413.
Meziane, H., Schaller, F., Bauer, S., Villard, C., Matarazzo, V., Riet, F., et al., 2015. An early postnatal oxytocin treatment prevents social and learning deficits in adult mice deficient for Magel2, a gene involved in Prader-Willi syndrome and autism. Biol. Psychiatry 78 (2), 85–94.
Milner, K.M., Craig, E.E., Thompson, R.J., Veltman, M.W., Thomas, N.S., Roberts, S., et al., 2005. Prader-Willi syndrome: intellectual abilities and behavioural features by genetic subtype. J. Child Psychol. Psychiatry 46 (10), 1089–1096.
Ninan, I., 2011. Oxytocin suppresses basal glutamatergic transmission but facilitates activity-dependent synaptic potentiation in the medial prefrontal cortex. J. Neurochem. 119 (2), 324–331.
Ripamonti, S., Ambrozkiewicz, M.C., Guzzi, F., Gravati, M., Biella, G., Bormuth, I., et al., 2017. Transient oxytocin signaling primes the development and function of excitatory hippocampal neurons. elife 6.
Schaaf, C.P., Gonzalez-Garay, M.L., Xia, F., Potocki, L., Gripp, K.W., Zhang, B., et al., 2013. Truncating mutations of MAGEL2 cause Prader-Willi phenotypes and autism. Nat. Genet. 45 (11), 1405–1408.
Schaller, F., Watrin, F., Sturny, R., Massacrier, A., Szepetowski, P., Muscatelli, F., 2010. A single postnatal injection of oxytocin rescues the lethal feeding behaviour in mouse newborns deficient for the imprinted Magel2 gene. Hum. Mol. Genet. 19 (24), 4895–4905.
Swaab, D.F., 1997. Prader-Willi syndrome and the hypothalamus. Acta Paediatr. 423, 50–54.
Swaab, D.F., Purba, J.S., Hofman, M.A., 1995. Alterations in the hypothalamic paraventricular nucleus and its oxytocin neurons (putative satiety cells) in Prader-Willi syndrome: a study of five cases. J. Clin. Endocrinol. Metab. 80 (2), 573–579.
Tacer, K.F., Potts, P.R., 2017. Cellular and disease functions of the Prader-Willi Syndrome gene MAGEL2. Biochem. J. 474 (13), 2177–2190.
Wijesuriya, T.M., De Ceuninck, L., Masschaele, D., Sanderson, M.R., Carias, K.V., Tavernier, J., et al., 2017. The Prader-Willi syndrome proteins MAGEL2 and necdin regulate leptin receptor cell surface abundance through ubiquitination pathways. Hum. Mol. Genet. 26 (21), 4215–4230.
Zhang, D., Isack, N.R., Glodowski, D.R., Liu, J., Chen, C.C., Xu, X.Z., et al., 2012. RAB-6.2 and the retromer regulate glutamate receptor recycling through a retrograde pathway. J. Cell Biol. 196 (1), 85–101.